Magnetic properties and amorphous-to-nanocrystalline transformation by thermal treatments in Fe84.3Si4P3B8Cu0.7 amorphous thin films

(Article begins on next page)

16 October 2023

UNIVERSITÀ DEGLI STUDI DI TORINO

Magnetic properties and amorphous-to-nanocrystalline transformation by thermal treatments in $Fe_{84.3}Si_4P_3B_8Cu_{0.7}$ amorphous thin films

Marco Coïsson[a], Patricio J. Viteri Villacis[b], Gabriele Barrera[a,b], Federica Celegato[a], Emauele Enrico[a], Paola Rizzi[b], Paola Tiberto[a], Franco Vinai[a], Gianluca Fiore[b], Livio Battezzati[b]

[a]*INRIM, Electromagnetics Division, strada delle Cacce 91, 10135 Torino (TO), Italy*
[b]*Università degli Studi di Torino, Chemistry Department, via P. Giuria 7, 10125 Torino (TO), Italy*

Abstract

Thin films of nominal composition $Fe_{84.3}Si_4P_3B_8Cu_{0.7}$ have been prepared by sputtering from ribbons of the same alloy. Their microstructure has been studied by means of X-ray diffraction, differential scanning calorimetry and transmission electron microscopy, and reveals a partly amorphous state in the as-prepared samples. Their magnetic properties are soft and comparable to those measured on rapidly quenched ribbons. After annealing in furnace at temperatures up to 400 °C, their soft magnetic properties are improved thanks to the development of a fully nanocrystalline state. Annealing at higher temperature causes the coarsening of the α-Fe like grains, the development of hard magnetic phases and an increase of the coercive field.

Keywords: Soft magnetic materials, Thin films, Amorphous to nanocrystalline transformation

1. Introduction

Nanocrystalline magnetic alloys have been extensively studied in the past decades because of their extremely important role in power applications, where high magnetic permeability and low coercivity are key requirements [1, 2]. More recently, FeSiB-based alloys have been proposed having a high value of saturation magnetisation ($B_S > 1.8$ T) [3, 4, 5, 6], which is a critical parameter to minimise energy losses when high power is required. In order to improve the nanocrystallinity of the alloy, Cu and P have been added to the base alloys, resulting in excellent magnetic softness [7].

In the information technology and in the sensors industry, the quest for excellent soft magnetic properties pushes the researchers to investigate similar alloys in thin films form [8, 9, 10], which are easier to integrate with electronics and existing Si processes. However, thin films are usually characterised by worse magnetic properties with respect to rapidly quenched ribbons having the same composition [11, 12].

In this paper, we investigate a high-B_S $Fe_{84.3}Si_4P_3B_8Cu_{0.7}$ alloy [3] in thin films form, obtained by sputtering starting from rapidly quenched ribbons. In the as-prepared conditions, the thin films are characterised by a nanocrystalline state that confers them good soft magnetic properties, comparable with those of the rapidly quenched ribbons. Subsequent thermal treatments in furnace further reduce the coercive field of the samples, leading to excellent soft magnetic properties in the studied films.

2. Experimental

The master alloy of nominal composition $Fe_{84.3}Si_4P_3B_8Cu_{0.7}$ has been prepared by arc-melting pre-alloyed Fe-B-Si and Fe-P with pure Cu element in Ar atmosphere with Ti and Zr getters. Moreover, Fe and Si pure elements were added in order to reach the required stoichiometry. Successively, ribbons having a width of 1 cm and a thickness of 30 ± 5 μm were obtained in a planar flow casting apparatus. Thin films were obtained by rf sputtering on glass substrates using targets made with the amorphous ribbons. By proper calibration of the deposition rate, samples have been prepared with a thickness of 100 and 200 nm.

The amorphous state of the ribbons was checked by DSC at the scanning rate of 20 K/min and their structure was examined by X-ray diffraction (XRD) with Cu K$_\alpha$ radiation and Bragg-Brentano geometry. The thin film structure was analysed using Grazing Incidence Diffraction (GID) with the same radiation. Transmission Electron Microscopy (TEM, Jeol 3010) was used to characterise the microstructure of as prepared and annealed films. TEM lamellae have been prepared by a focussed ion beam (FIB) process in a FEI Quanta 3D dual beam microscope (Fig. 1). The region of interest is first coated with a protective Pt deposition obtained with a gas injection system (Fig. 1 a). Then, trenches are milled with the ion beam delimiting the lamellae (Fig. 1 b). Once free on all sides but one, the lamella is attached to a nano manipulator and detached from the thin film (Fig. 1 c). Finally, the lamella is attached to a lift-out grid and thinned with the ion beam to the desired thickness adequate for TEM imaging (Fig. 1 d).

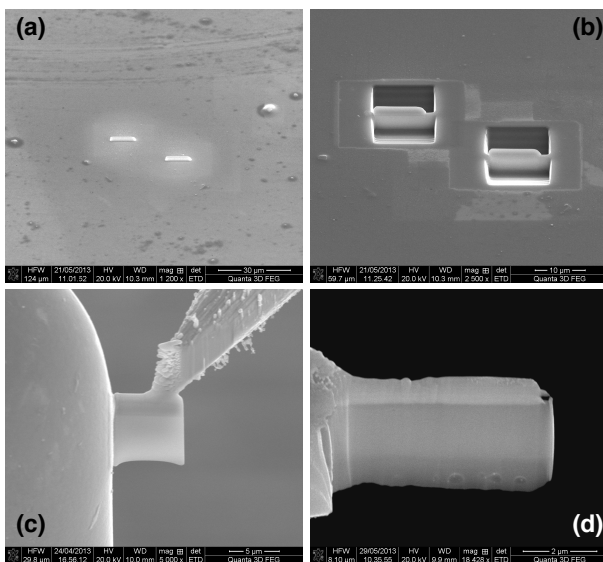Selected samples have been annealed in furnace in vacuum (base pressure

Figure 1: Preparation of a TEM lamella. (a) Pt deposition on top of the area that will be cut into a lamella. (b) Milling of the trenches around the lamellae. (c) Detachment of a lamella with a nano manipulator. (d) Thinned lamella attached to a lift-out grid.

$\approx 1 \cdot 10^{-5}$ mbar) at temperatures up to 550 °C for 1 h. Room temperature magnetisation measurements have been performed with an alternating gradient field magnetometer (AGFM) with the magnetic field applied in the sample plane. Magnetisation measurements as a function of temperature have been performed with a vibrating sample magnetometer (VSM) equipped with a furnace operating in continuous Ar flow, at temperatures up to 800 °C, with the field applied in the sample plane.

3. Results and discussion

Structural characterisation. $Fe_{84.3}Si_4P_3B_8Cu_{0.7}$ as quenched ribbons are constituted by a fraction of amorphous phase, as can be seen in the XRD patterns of the air and wheel side reported in Fig. 2. Inhomogeneities are

4

present along the ribbon, due to the low glass forming ability of this alloy [3]. The amount of crystals, identified as α-Fe type phase, increases from wheel (Fig. 2 a) to air side (Fig. 2 b). Two crystallisation peaks are present in the DSC trace with onset temperatures equal to 388 °C and 550 °C, respectively. The first exotherm is due to the partial crystallisation of the amorphous matrix into α-Fe type phase. The second one is related to the precipitation, from the remaining amorphous phase, of unindexed compounds containing boron and phosphorous which, however, are detrimental for soft magnetic properties. Therefore, all subsequent thermal treatments will not exceed the 550 °C limit.
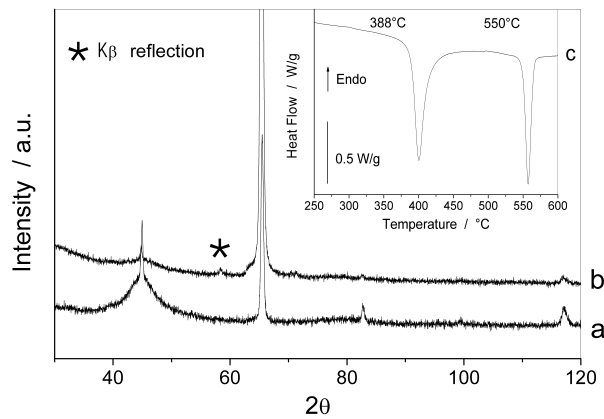
Figure 2: Diffraction patterns and DSC trace of an as-quenched ribbon: (a) wheel side and (b) air side.

The film samples structure was checked by GID and TEM analyses. In the as prepared 100 nm film (Fig. 3 a), a small peak appears superimposed to the amorphous halo in the GID analysis related to the presence of a α- Fe type phase embedded in the amorphous phase. This is confirmed by TEM analysis that show crystals elongated in the film deposition direction, with

5

average dimensions ranging from 10 nm to 30 nm of width and up to 90 nm of length (Fig. 4 a). A larger fraction of amorphous phase is observed in this sample, with respect to the as quenched ribbons, both by GID and TEM. In the 200 nm as prepared film, the microstructure appears similar to the 100 nm thick sample, as evidenced using GID (Fig. 3 b). Both films appear homogeneous in structure. Therefore, inhomogeneities observed in the ribbon are not detrimental for its use as a target for the production of thin films.
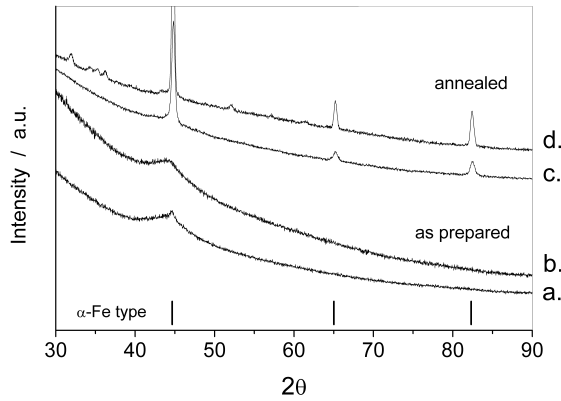
Figure 3: Grazing Incidence Diffraction pattern of: a) 100 nm film as prepared; b) 200 nm film as prepared; c) 100 nm film heated up to 550 °C; d) 200 nm film heated up to 550 °C.

In order to identify suitable temperatures for annealing, 3x3 mm^2 samples cut from the ribbon and from the 100 nm and 200 nm thin films have been submitted to a magnetisation vs. temperature measurement in a VSM equipped with a furnace, under the application of a magnetic field of 1000 Oe and with a heating rate of 2 K/min. The results are reported in Fig. 5. Starting from room temperature, the magnetisation decreases because of

6

Figure 4: TEM bright field images and corresponding SAED (in inset) of $Fe_{84.3}Si_4P_3B_8Cu_{0.7}$: a) 100 nm as prepared film; b) 100 nm film heated up to 550 °C.

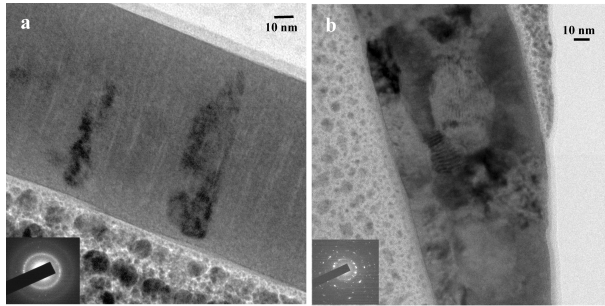the progressive approach to the Curie temperature of the amorphous phase. In thin films, at temperatures between 280 and 350 °C the magnetisation increases, because of the onset of crystallisation processes: some of the Fe atoms that were dispersed in the amorphous matrix determine the nucleation of new α-Fe like crystals and/or the growth of existing ones, thus causing an increase of the magnetic moment of the sample. The same effect is observed in ribbons at slightly higher temperatures. The onset of crystallisation occurs at temperatures that are consistent with DSC data (Fig. 2) considering the different heating rates in the two experiments. As the temperature is further increased, this process continues until the Curie temperature of the α-Fe phase is reached (≈ 770 °C as shown for the ribbon sample in Fig. 5). Indeed, while the Curie temperature of the amorphous phase, although it can only be estimated by extrapolation from the initial part of the M vs. T curves, seems the same for all samples, a significant reduction of the Curie temperature of the α-Fe like phase is observed. This reduction suggests that the amount of α-Fe is reduced in the film possibly because of oxidation. Reaction with either some residual oxygen in the annealing atmosphere or the

glass substrate is unavoidable. According to [13], the observed Curie temperatures of the α-Fe like crystals are compatible with Si atomic concentrations between 11% for the 100 nm thin film and 16 % for the 200 nm one. It is important to observe that the Si concentration in the α-Fe crystals of the as-prepared samples or annealed at temperatures lower than about 500 °C should be compatible with the nominal composition of the alloy, as suggested by the invariance of the Curie temperature of the amorphous phase of films of different thickness.
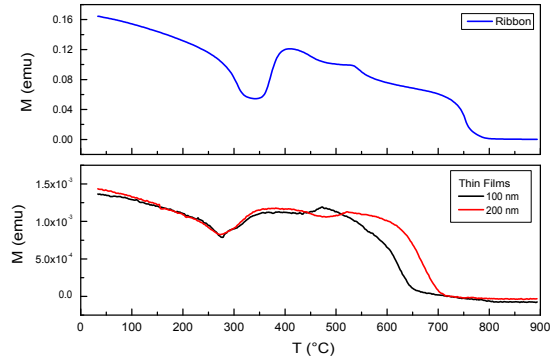

Figure 5: M vs. T measurements on selected samples (ribbon, top layer, and 100 and 200 nm thin films, bottom layer) under an applied field of 1000 Oe.

Following the results of Fig. 5, thin film samples were heated at 300, 400, 500 and 550 °C. The structure of the samples annealed at the highest temperature was determined by TEM and GID analyses, as shown in Fig. 4 b and Fig. 3 c and d. In both film samples the amorphous phase is completely crystallised in α-Fe type phase (Fig. 3 c and d). A limited amount of an unindexed phase is detected in the peaks at low angle in Fig. 3 d. As the annealing at 550 °C is very close to the onset of the second crystallisation

8

process (see the DSC trace in Fig. 2), this minority phase is difficult to detect in both XRD spectra, especially in the one of the annealed 100 nm film. This finding is confirmed by TEM analysis (Fig. 4 b) of the 100 nm film, in which a completely crystallised sample is observed, composed by crystals of the α-Fe type phase (SAED reported in the inset of Fig. 4 b). The average crystal size was determined from TEM images to be about 40 nm.

Magnetic properties. Room temperature hysteresis loops of the as-quenched ribbon and as-prepared 100 and 200 nm thin films are shown in Fig. 6 a and b respectively. Both film samples are characterised by a fast approach to saturation and a low coercive field, although the 200 nm thick sample is slightly harder. This is consistent with GID analysis (Fig. 3), that identifies in this sample a higher degree of amorphous phase which corresponds to a larger coercivity: in fact, the presence of fewer nanocrystals leads to a reduced effectiveness of the anisotropy averaging out. Conversely, the 100 nm thick sample has a coercive field of the order of $1-2$ Oe, which is comparable with the one measured on the rapidly solidified ribbons [3] (see Fig. 6). As the film crystals are elongated along the film growth direction, the demagnetising coefficient overwhelms any anisotropy that may arise from their oblong shape. Conversely, for the ribbon the approach to saturation is slower than for the films: this can be attributed to the higher value of the demagnetising field in the in-plane directions with respect to films, as ribbons with a comparable size adequate for AGFM investigation (i.e. not larger than 3×3 mm^2) are much thicker than thin films [14].

After having been submitted to furnace annealing, the hysteresis loops of the thin film samples have been measured again at room temperature with
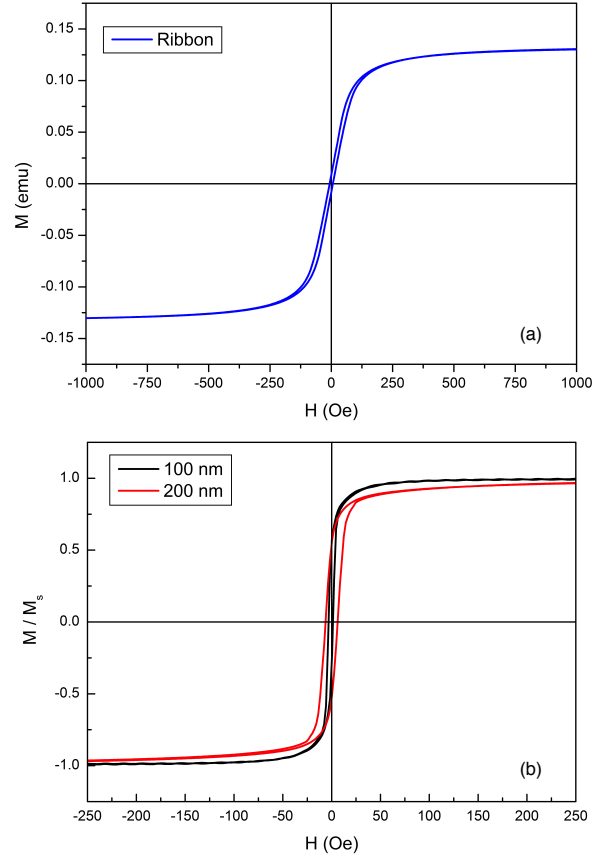
Figure 6: Room temperature hysteresis loops of (a) as-quenched ribbon and (b) as-prepared 100 nm and 200 nm thin films.

the AGFM to investigate the effect of the microstructure evolution on their magnetic properties. The results are summarised in Fig. 7.

With respect to the as-prepared films, annealing at 300 and 400 °C causes a reduction of the coercive field to values < 1 Oe (below the detection limit with AGFM measurements) for the 100 nm thick sample, which are even better than what observed in the rapidly quenched ribbons. In agreement with the data reported in Fig. 5 and with the help of the TEM results on
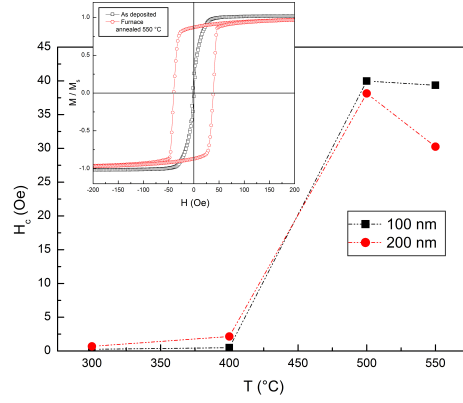
Figure 7: Coercive field evolution as a function of temperature in furnace annealed 100 nm and 200 nm films. Inset: comparison of the hysteresis loops of an as-prepared and a 550 C° annealed 100 nm thin film.

the as-prepared 100 nm sample, it is suggested that the low-temperature annealing is responsible for an increase in the number of small α-Fe like crystals per unit volume, effectively averaging out the local magnetic anisotropy, although the estimated crystal size is larger than the value required for an optimal application of the Random Anisotropy Model [15]. Additionally, a relaxation of the quenched in stresses during sample deposition may also contribute to the reduction of the coercive field.

When the annealing temperature is $\geqslant$ 500 °C, a significant increase of the coercive field is observed. According to the TEM observations (Fig. 4), at these temperatures a fully crystalline sample is obtained, but the increased crystals size is too large for the Random Anisotropy Model to be truly effective. Moreover, XRD (see Fig. 3) suggests that a small fraction of unindexed compounds may have developed in the thin film samples annealed at the highest temperature. This phase is characterised by harder magnetic

properties [16] and may account for the resulting remarkable loop shape variation shown in the inset of Fig. 7 for the 100 nm thick film annealed at 550 °C.

4. Conclusions

Thin films of nominal composition $Fe_{84.3}Si_4P_3B_8Cu_{0.7}$ have been successfully obtained by sputtering from rapidly quenched ribbons of the same alloy. The as-prepared films, with a thickness of 100 and 200 nm, are characterised by the presence of numerous α-Fe like grains and a soft magnetic behaviour. In the as-prepared state, the thin films have magnetic properties that are comparable with those observed on the rapidly quenched ribbons.

Thermal treatments in furnace have induced a softening of the magnetic properties of the films, with a reduction of their coercive field below 1 Oe for annealing temperatures up to 400 °C, thanks to the development of a fully nanocrystalline state. Annealing at higher temperatures causes a coarsening of the grains and the development of a minority hard phase most probably containing boron and phosphorus, that is responsible for a significant increase of the coercive field up to $35 - 40$ Oe. The magnetic results are supported by XRD and TEM observations of the thin films microstructure in the as-prepared and annealed conditions.

References

[1] M.E. McHenry, M.A. Willard, and D.E. Laughlin, Prog. Mater Sci. **44** (1999) 291

[2] A. Makino A, T. Hatanai, Y. Naitoh, T. Bitoh, A. Inoue, and T. Masumoto, IEEE Trans. Magn. **33(5)** (1997) 3793

[3] A.Makino, H.Men, T.Kubota, K.Yubuta, A.Inoue, Materials Transactions, **50** (2009) 204 - 209

[4] M. He, L. Cui, T. Kubota, K. Yubuta, A. Makino, A. Inoue, Materials Transaction **50** (2009) 1330 - 1333

[5] T. Kubota, A. Makino, A. Inoue, J. Alloy and Compd. **509S** (2011) S416 - S419

[6] M. Ohta, Y. Yoshizawa, J. Phys. D: Appl. Phys. **44** (2011) 064004

[7] F. Kong, A. Wang, X. Fan, H. Men B. Shen, G. Xie, A. Makino, A. Inoue, J. Appl. Phys. **109** (2011) 07A303

[8] U.B. Arnalds, E.Th. Papaioannou, T.P.A. Hase, H. Raanaei, G. Andersson, T.R. Charlton, S. Langridge, B. Hjörvarsson, Phys. Rev. B **82(14)** (2010) 144434

[9] J.U. Cho, D.K. Kim, R.P. Tan, S. Isogami, M. Tsunoda, M. Takahashi and Y.K. Kim, IEEE Trans. Magn. **45(6)** (2009) 2364

[10] M. Coïsson, F. Celegato, E.S. Olivetti, P. Tiberto, F. Vinai, S.N. Kane, E.A. Gan'shina, A.I. Novikov, N.S. Perov, J. Alloy Compd. **509** (2011) 4688-4695

[11] J. Füzer, J. Balcierski, P. Matta, A. Zorkovská and A. Zelenáková, J. Phys. IV France **08** (1998) Pr2-127-Pr2-130

[12] F. Celegato, M. Coisson, P. Tiberto, F. Vinai, M. Baricco, Phys. Status Solidi C **8** (2011) 3070-3073

[13] Landolt-Börnstein, *Magnetic properties of metals*, Group III, Volume 19, subvolume I-1, ISSN 0942-7988, Springer-Verlag Berlin Heidelberg (1994), 50

[14] A. Aharoni, J. Appl. Phys. **83** (1998) 3432

[15] G. Herzer, *IEEE Trans. Magn.* **26(5)** (1990) 1397-1402

[16] V. de Manuel and R.P. del Real, J. Phys. D:Appl. Phys. **41** (2008) 085001